18th International Conference on Information Fusion
Washington, DC - July 6-9, 2015

Passive Tracking of Underwater Acoustic Sources with Sparse Innovations

Pedro A. Forero, Paul Baxley, and Logan Straatemeier
SPAWAR Systems Center Pacific, San Diego, CA 92152, United States
Email: {pedro.a.forero;paul.baxley;logan.straatemeier}@navy.mil

***Abstract*—Tracking acoustic sources via passive sonar is a challenging task common to several underwater monitoring and surveillance systems. Classical tracking approaches based on matched-field tracking and Kalman filtering techniques are impractical due to the their large computational and storage requirements. This work uses sparse-signal modeling tools to develop a computationally-affordable broadband tracking algorithm for an entire source-location map (SLM). Spectral data from multiple frequency bands are processed coherently so as to unambiguously agree on the source locations across frequencies. The tracking problem is cast so that the sparsity inherent in the SLM and in the SLM-innovations can be exploited. A numerical solver based on the proximal gradient method and the alternating directions method of multipliers is developed for SLM estimation. Numerical tests on real data illustrate their performance.**

***Index Terms*—matched-field tracking, underwater acoustic source localization, sparsity, proximal gradient methods**

I. INTRODUCTION

Passive sonar enables monitoring and surveillance systems to operate without radiating sound into the water; hence, it is often employed in applications where concealment and low environmental impact are desired. Acoustic data collected over time can be used for sketching source tracks by, for example, plotting source-location estimates over time [1], [11]. Tracking capitalizes on the *temporal* structure inherent to source tracks, which are always constrained by the kinematic features of the source, to improve source-location estimates. However, using classical tracking methods, such as Kalman filtering, to develop a passive acoustic tracker poses significant computational challenges [8], [11].

Matched-field tracking (MFT) is a passive acoustic tracking approach that builds on a generalized underwater beamforming technique called matched-field processing (MFP) [5], [15]. MFP postulates a grid of tentative source locations and relies on an acoustic propagation model to obtain model-predicted acoustic pressures, hereafter referred to as *replicas*, at an array of hydrophones. Replicas are "matched" to acoustic measurements collected at the array to construct a surface that summarizes the acoustic-power estimates across all grid locations [1]. MFT relies on a sequence of ambiguity surfaces obtained at consecutive time intervals for constructing tracks. Note that these ambiguity surfaces are constructed independently from each other without exploiting their temporal correlation. Then, MFT constructs a graph connecting grid points on consecutive ambiguity surfaces. Each possible path over this graph connecting the initial and final ambiguity surface is scored based on, e.g., its average ambiguity surface value, and the path with the largest score serves as a track estimate [9], [14]. Unfortunately, the complexity of MFT grows quickly with the size of the grid and the number of ambiguity surfaces used. Constraints obtained form the source's kinematics are often used to limit the number of tracks to be explore.

Sparsity-driven Kalman-filter approaches can be used for tracking acoustic sources over a grid [8]. In these approaches, the entire grid takes the place of the state variable. It is presumed that only a few entries of the grid, that is, those corresponding to the locations of the sources, take nonzero values and, thus, the state variable is considered to be sparse. Unfortunately, the high dimensionality of the grid renders impractical any tracker that computes the full covariance matrix of the state variable.

Our broadband tracking approach builds on the sparsity-driven framework outlined above. It aims to construct *sparse* source location maps (SLMs), one per frequency, while exploiting their temporal dependence. Only those grid points whose locations correspond to a source location take a nonzero value, which represents the complex-valued acoustic signature of the source. The tracker guarantees the support of the various grids to coincide, thereby assuring unambiguous source-location estimates across frequencies. Different from Kalman trackers, our tracker relies on prior SLM estimates only.

An *innovation* is defined as a change in the support of consecutive SLMs. The proposed tracker controls the number of innovations allowed to occur. It is assumed that innovations are sparse, and thus few sources change their location between consecutive SLMs. Our tracking framework extends that proposed by Charles et al. in [6] by introducing a broadband tracker in which source-location information is shared across frequencies [10]. The resulting complex-valued optimization problem features a compounded regularizer that encourages sparse SLMs and sparse innovations. Iterative solvers based on a combination of the proximal gradient (PG) method and the alternating direction method of multipliers (ADMM) are developed. Numerical tests on real data illustrate the performance of the proposed tracking algorithm.

II. PRELIMINARIES

Consider K broadband acoustic sources radiating sound underwater. Although all sources are presumed to be mobile,

This work was funded by the Naval Innovative Science and Engineering Program at the Space and Naval Warfare Systems Center Pacific.

thus justifying the dependence of their locations $\{\mathbf{r}_k(\tau)\}_{k=1}^K$ on the time $\tau \in \mathbb{N}$, no assumptions about their kinematics are made. Each $\mathbf{r}_k(\tau) \in \mathbb{R}^d$ is given in cylindrical coordinates comprising the source's range, depth (with respect to the sea surface), and azimuth, with $d \in \{1, 2, 3\}$. An array with N hydrophones of known, but arbitrary, geometry is used to collect a time series of acoustic pressure vectors $\{\mathbf{y}(\tau) \in \mathbb{R}^N : \tau \in \mathbb{N}\}$ with entries $[\mathbf{y}(\tau)]_n \in \mathbb{R}$ denoting the acoustic pressure measured by the n-th hydrophone in the array at time τ. Note that although our framework is agnostic to the specific geometry of the array, its geometry affects our definition of source location. For instance, data gathered with an array that features horizontal aperture but no vertical aperture provides information about the sources' azimuth only ($d = 1$), whereas data gathered with an array featuring vertical and horizontal aperture provides information about the sources' range, depth, and azimuth ($d = 3$) [11, Ch. 10].

Localization and tracking algorithms that use $\{\mathbf{y}(\tau)\}$ directly are often challenged by the high sampling and computational requirements necessary to reconstruct the channel impulse responses between the source locations and the hydrophones [7]. Instead, this work develops a frequency-based passive-tracking approach that does not require estimating the channel impulse responses. To this end, $\{\mathbf{y}(\tau) : \tau \in \mathbb{N}\}$ is *sequentially* processed per hydrophone by computing short-time Fourier transforms (STFT) of length T_0. Consecutive blocks of the acoustic-pressure time series data can overlap and be scaled (per hydrophone) by a carefully chosen window function so as to reduced sidelobes and decrease the variability in the spectrum of the acoustic pressure series due to noise [11, Ch. 10]. Fourier coefficients at F frequencies $\{\omega_f\}_{f=1}^F$ across the N hydrophones are gathered in $\mathbf{Y}^m := [\mathbf{y}_1^m, \ldots, \mathbf{y}_F^m] \in \mathbb{C}^{N\times F}$, where $[\mathbf{Y}^m]_{n,f} \in \mathbb{C}$ denotes the Fourier coefficient corresponding to ω_f for the n-th hydrophone in the m-th STFT block.

Each $\mathbf{y}_f^m$ is modeled as

$$\mathbf{y}_f^m = \sum_{k=1}^{K} s_{k,f}^m \bar{\mathbf{p}}_{k,f} + \boldsymbol{\epsilon}_f^m,\ \forall m, f \tag{1}$$

where $s_{k,f}^m \in \mathbb{C}$ denotes the Fourier coefficient at ω_f of the acoustic signature of the k-th source obtained by the m-th STFT, $\bar{\mathbf{p}}_{k,f} \in \mathbb{C}^N$ the model-predicted Fourier coefficient vector at the array for the k-th source at frequency ω_f normalized so that $\|\bar{\mathbf{p}}_{k,f}\|_2 = 1$, and $\boldsymbol{\epsilon}_f^m$ the spectral components of the array's measurement noise at ω_f for the m-th STFT block. The replicas $\bar{\mathbf{p}}_{k,f}$'s are obtained using a model that characterizes the acoustic propagation environment and the geometry of the array [11, Ch. 10].

Given K, the goal of the *spectral* passive-acoustic tracking problem is to recursively estimate the locations $\{\mathbf{r}_k(\tau_M)\}_{k=1}^K$ of the acoustic sources at $\tau_M = \lfloor(1-\alpha)T_0 M\rfloor$ based on the sequence of Fourier coefficient matrices $\{\mathbf{Y}^m\}_{m=0}^M$, where $\alpha \in [0, 1)$ denotes percentage of overlap between consecutive STFT blocks. Note that here τ_M denotes the time index corresponding to the beginning of the M-th temporal acoustic-data block. Even if all $s_{k,f}^m$'s were known, finding $\{\mathbf{r}_k(\tau_M)\}_{k=1}^K$ based on (1) is challenging due to the nonlinear relationship between each $\mathbf{r}_k(\tau_M)$ and its corresponding $\bar{\mathbf{p}}_{k,f}$, $\forall f$, which in most cases is not available in closed form.

III. Broadband sparsity-driven source tracking

A model for the $\mathbf{y}_f^m$'s that alleviates the challenges associated with the nonlinearities inherent to (1) is proposed in this section. Let $\mathcal{G} := \{\mathbf{r}_g \in \mathbb{R}^d\}_{g=1}^G$, with $G \gg \max\{N, KF\}$, denote a grid of tentative source locations over the region of interest. Each $\mathbf{y}_f^m$ is now modeled as

$$\mathbf{y}_f^m = \sum_{g=1}^{G} s_{g,f}^m \mathbf{p}_{g,f} + \boldsymbol{\epsilon}_f^m,\ \forall f \tag{2}$$

where $\mathbf{p}_{g,f}$ denotes the normalized replica, i.e., $\|\mathbf{p}_{g,f}\|_2 = 1$, for a source located at $\mathbf{r}_g \in \mathcal{G}$, and $s_{g,f}^m$ the unknown Fourier coefficient associated to the acoustic signature at frequency ω_f for a source located at $\mathbf{r}_g$. Note that (2) tacitly assumes that the acoustic sources are located exactly on some $\mathbf{r}_g \in \mathcal{G}$. Since $G \gg KF$, most of the $s_{g,f}^m$'s are expected to be zero at any given m. Only coefficients $s_{g,f}^m$ that correspond to the location of the acoustic sources take nonzero values, and thus their corresponding replicas participate in (2). All $s_{g,f}^m$'s associated to locations where acoustic sources are absent are set to zero.

From the vantage point of (2), finding estimates for $\{\mathbf{r}_k(\tau_m)\}_{k=1}^K$ is tantamount to identifying the locations in $\mathcal{G}$ corresponding to the nonzero $s_{g,f}^m$'s. Let $(\cdot)'$ denote the transpose operator and $\mathbf{s}_f^m := [s_{1,f}^m, \ldots, s_{G,f}^m]'\ \forall f$. Once an estimate for $\mathbf{S}^m := [\mathbf{s}_1^m, \ldots, \mathbf{s}_F^m] \in \mathbb{C}^{G\times F}$ is available, one can construct the broadband SLM. This can be done by, e.g., plotting the pairs $(\mathbf{r}_g, \|\boldsymbol{\varsigma}_g^m\|_2)$ for all $\mathbf{r}_g \in \mathcal{G}$, where $\boldsymbol{\varsigma}_g^m := [s_{g,1}^m, \ldots, s_{g,F}^m]' \in \mathbb{C}^F$ comprises the entries of the g-th row of $\mathbf{S}^m$. Source location estimates $\{\hat{\mathbf{r}}_k(\tau_m)\}_{k\in\mathcal{K}}$ indexed by the index-set $\mathcal{K} \subset \{1, \ldots, K\}$ are given by the locations that correspond to the K-largest entries in the SLM, i.e., $\mathcal{K} \in \arg\max_{|\mathcal{K}|=K} \sum_{\kappa\in\mathcal{K}} \|\boldsymbol{\varsigma}_\kappa^m\|_2$.

A localization algorithm that exploits the inherent *sparse* structure of $\mathbf{S}_m$ was proposed in [10]. This approach estimates $\mathbf{S}^m$ using $\{\mathbf{y}_f^m\}_{f=1}^F$ only, while enforcing a common-support across all its columns $\{\mathbf{s}_f^m\}_{f=1}^F$. The requirement on the support of $\mathbf{S}^m$ is justifiable since it is assumed that the acoustic signal radiated by each source spans all $\{\omega_f\}_{f=1}^F$. Nevertheless, such an estimator for $\mathbf{S}^m$ does not capture the temporal dependencies inherent to source motion which are due to the physical constraints on the kinematics of the acoustic sources.

A. Sparsity-driven tracking with sparse innovations

In this section, an iterative estimator for $\mathbf{S}^m$ is proposed. The distinctive feature of this estimator is that it uses the previously estimated $\mathbf{S}^{m-1}$ to capture the temporal evolution of the source locations. At τ_m, $\mathbf{S}^m$ is obtained as the solution of the following regularized least-squares problem

$$\min_{\mathbf{S}\in\mathbb{C}^{G\times F}} \frac{1}{2}\sum_{f=1}^{F}\|\mathbf{y}_f^m-\mathbf{P}_f\mathbf{s}_f\|_2^2+\sum_{g=1}^{G}\left[\mu\|\boldsymbol{\varsigma}_g\|_2+\lambda\|\boldsymbol{\varsigma}_g-\boldsymbol{\varsigma}_g^{m-1}\|_2\right] \tag{3}$$

where $\mathbf{S} := [\mathbf{s}_1,\ldots,\mathbf{s}_F]$, $\boldsymbol{\varsigma}_g'$ the g-th row of $\mathbf{S}$, $\mathbf{P}_f := [\mathbf{p}_{1,f},\ldots,\mathbf{p}_{G,f}] \in \mathbb{C}^{N\times G}$ the matrix of replicas for ω_f, and $\mu,\lambda > 0$ tuning parameters. The regularization term in (3) encourages both group sparsity on the rows of $\mathbf{S}^m$ and sparsity in the innovations, that is, changes in the support between the SLMs at τ_{m-1} and τ_m.

The first term of the regularizer promotes our desiderata of common support for the columns of $\mathbf{S}^m$. The tuning parameter μ controls the number of nonzero rows in $\mathbf{S}^m$. The second term of the regularizer captures temporal information related to the previous SLM via the $\boldsymbol{\varsigma}_g^{m-1}$'s. The number of innovations allowed to occur between τ_{m-1} and τ_m is controlled via λ.

As stated in the following proposition, (3) can be written as a real-valued convex optimization problem after representing all complex-valued variables by the direct sum of their real and imaginary parts. Before stating the proposition, let us introduce the following notation $\breve{\mathbf{y}}_f^m := [\mathrm{Re}(\mathbf{y}_f^m)',\mathrm{Im}(\mathbf{y}_f^m)']'$, $\breve{\mathbf{s}}_f := [\mathrm{Re}(\mathbf{s}_f)',\mathrm{Im}(\mathbf{s}_f)']'$, $\breve{\mathbf{S}} := [\breve{\mathbf{s}}_1,\ldots,\breve{\mathbf{s}}_F]$, and

$$\breve{\mathbf{P}}_f := \begin{bmatrix} \mathrm{Re}(\mathbf{P}_f) & -\mathrm{Im}(\mathbf{P}_f) \\ \mathrm{Im}(\mathbf{P}_f) & \mathrm{Re}(\mathbf{P}_f) \end{bmatrix} \tag{4}$$

where $\mathrm{Re}(\cdot)$ ($\mathrm{Im}(\cdot)$) denotes the real-part (imaginary-part) operator. Matrix $\breve{\mathbf{S}}$ can be alternatively viewed in terms of its rows as $\breve{\mathbf{S}} = [\breve{\varsigma}_1,\ldots,\breve{\varsigma}_{2G}]'$ where the first (last) G rows correspond to the real (imaginary) parts of the rows of $\mathbf{S}$.

Proposition 1: The minimum of (3) is equal to that of the following convex optimization problem

$$\breve{\mathbf{S}}^m = \arg\min_{\breve{\mathbf{S}}\in\mathbb{R}^{2G\times F}} \frac{1}{2}\sum_{f=1}^{F}\|\breve{\mathbf{y}}_f^m-\breve{\mathbf{P}}_f\breve{\mathbf{s}}_f\|_2^2+\mu\sum_{g=1}^{G}\|\mathbf{v}_g\|_2 + \lambda\sum_{g=1}^{G}\|\breve{\mathbf{v}}_g-\breve{\mathbf{v}}_g^{m-1}\|_2 \tag{5}$$

where $\breve{\mathbf{v}}_g := [\breve{\varsigma}_g',\breve{\varsigma}_{g+G}']' \in \mathbb{R}^{2F}$ ($\breve{\mathbf{v}}_g^{m-1}$) corresponds to the direct sum of the real and imaginary parts of ς_g (ς_g^{m-1}). Moreover, the minimizer $\mathbf{S}^m$ of (3) is given in terms of $\breve{\mathbf{S}}^m$ as $\mathbf{S}^m = \breve{\mathbf{S}}^m_{1:G} + \mathrm{j}\breve{\mathbf{S}}^{\mathrm{m}}_{\mathrm{G+1:2G}}$, where $\mathrm{j} := \sqrt{-1}$ and $\breve{\mathbf{S}}^m_{g_1:g_2} = [\breve{\varsigma}_{g_1},\ldots,\breve{\varsigma}_{g_2}]'$, for all $g_1 \le g_2$, $g_1,g_2 \in \{1,\ldots,G\}$.

Although (5) is a convex optimization problem that can be solved via, e.g., interior point methods, such solver entails high computational complexity due to the large dimensionality of $\breve{\mathbf{S}}$ and fails to exploit the sparse structure of $\breve{\mathbf{S}}$. The ensuing section presents a PG solver for (5) that exploits its sparse structure.

IV. Sparse tracking via PG

In this section a PG algorithm for solving (5) while exploiting its sparse structure is developed. Problem (5) can be written as $\min_{\breve{\mathbf{S}}}\ h(\breve{\mathbf{S}})+\theta(\breve{\mathbf{S}})$, where $h(\breve{\mathbf{S}}) := \frac{1}{2}\sum_{f=1}^{F}\|\breve{\mathbf{y}}_f^m - \breve{\mathbf{P}}_f\breve{\mathbf{s}}_f\|_2^2$ denotes the continuously differentiable portion of the cost, and $\theta(\breve{\mathbf{S}}) := \mu\sum_{g=1}^{G}\|\breve{\mathbf{v}}_g\|_2 + \lambda\sum_{g=1}^{G}\|\breve{\mathbf{v}}_g - \breve{\mathbf{v}}_g^{m-1}\|_2$ the nondifferentiable portion of the cost. Note that the gradient of $h(\breve{\mathbf{S}})$ is Lipschitz continuous with Lipschitz constant $L_h := \max_{f=1,\ldots,F}\sigma_{\max}(\mathbf{P}_f'\mathbf{P}_f)$, where $\sigma_{\max}(\mathbf{P}_f'\mathbf{P}_f)$ denotes the largest singular value of $\mathbf{P}_f'\mathbf{P}_f$. That is, $\|\nabla h(\breve{\mathbf{S}}_1)-\nabla h(\breve{\mathbf{S}}_2)\|_2 \le L_h\|\breve{\mathbf{S}}_1-\breve{\mathbf{S}}_2\|_F$, where $\nabla h(\breve{\mathbf{S}}_l)$ denotes the gradient of h with respect to $\breve{\mathbf{S}}$ evaluated at $\breve{\mathbf{S}}_l$.

The PG method can be interpreted as a majorization-minimization method relying on a majorizer $H(\breve{\mathbf{S}};\mathbf{Z})$ for h, where $\mathbf{Z} := [\mathbf{z}_1,\ldots,\mathbf{z}_F] \in \mathbb{R}^{2G\times F}$ is an auxiliary matrix. The majorizer H satisfies: (i) $H(\breve{\mathbf{S}};\mathbf{Z}) \ge h(\breve{\mathbf{S}})$, $\forall\breve{\mathbf{S}}$; and, (ii) $H(\breve{\mathbf{S}};\mathbf{Z}) = h(\breve{\mathbf{S}})$ for $\mathbf{Z} = \breve{\mathbf{S}}$. The specific H used is

$$H(\breve{\mathbf{S}};\mathbf{Z}) := h(\mathbf{Z})+\sum_{f=1}^{F}\nabla h_f(\mathbf{z}_f)'(\breve{\mathbf{s}}_f-\mathbf{z}_f)+\frac{L_h}{2}\|\breve{\mathbf{S}}-\mathbf{Z}\|_F^2 \tag{6}$$

where $h_f(\breve{\mathbf{s}}_f) := 1/2\|\breve{\mathbf{y}}_f^m - \breve{\mathbf{P}}_f\breve{\mathbf{s}}_f\|_2^2$, and $\nabla h_f(\mathbf{z}_f)$ denotes the gradient of h_f with respect to $\breve{\mathbf{s}}_f$ evaluated at $\mathbf{z}_f$. That (6) satisfies conditions (i) follows from the fact that the gradient of h is Lipschitz continuous [3, Prop. A.24], and that it satisfies (ii) follows after setting $\mathbf{Z} = \breve{\mathbf{S}}$ in (6). With j denoting the iteration index, the PG algorithm iteratively solves

$$\breve{\mathbf{S}}^m[j] = \arg\min_{\breve{\mathbf{S}}}\left[H(\breve{\mathbf{S}};\breve{\mathbf{S}}^m[j-1])+\theta(\breve{\mathbf{S}})\right]. \tag{7}$$

From an algorithmic point of view, it is convenient to write H as a function of the $\breve{\mathbf{v}}_g$'s. After performing some algebraic manipulations on H and dropping al terms independent of $\breve{\mathbf{S}}$, (7) can be written as

$$\breve{\mathbf{S}}^m[j] = \arg\min_{\breve{\mathbf{S}}}\left[\sum_{g=1}^{G}\frac{L_h}{2}\left\|\breve{\mathbf{v}}_g-\mathbf{w}_g^m[j-1]\right\|_2^2+\theta(\breve{\mathbf{S}})\right] \tag{8}$$

where

$$\mathbf{w}_g^m[j-1] := \breve{\mathbf{v}}_g^m[j-1]-(1/L_h)\mathbf{d}_g^m[j-1] \tag{9}$$

is a gradient-descent step, with step-size $1/L_h$, for the g-th row of $\breve{\mathbf{S}}$, and the entries of $\mathbf{d}_g^m[j-1]$, which correspond to those of the gradient of h_f with respect to $\breve{\mathbf{v}}_g$, are

$$[\mathbf{d}_g^m[j-1]]_f = \begin{cases} -\breve{\mathbf{p}}_{g,f}'\mathbf{r}_f^m[j-1], & f=1,\ldots,F \\ -\breve{\mathbf{p}}_{g+G,f}'\mathbf{r}_f^m[j-1], & f=F+1,\ldots,2F \end{cases} \tag{10a}$$

where $\mathbf{r}_f^m[j-1] := \breve{\mathbf{y}}_f - \breve{\mathbf{P}}_f\breve{\mathbf{s}}_f^m[j-1]$. Problem (8) is often called the proximal operator of θ with parameter $1/L_h$.

Problem (8) is decomposable across $\breve{\mathbf{v}}_g$'s. Thus, per iteration j, the PG update in (7) can be performed in parallel for every pair of rows of $\breve{\mathbf{S}}$ comprised in each $\breve{\mathbf{v}}_g$ via

$$\breve{\mathbf{v}}_g^m[j] = \arg\min_{\breve{\mathbf{v}}_g}\left[\frac{L_h}{2}\left\|\breve{\mathbf{v}}_g-\mathbf{w}_g^m[j-1]\right\|_2^2 +\mu\|\breve{\mathbf{v}}_g\|_2+\lambda\|\breve{\mathbf{v}}_g-\breve{\mathbf{v}}_g^{m-1}\|_2\right] \tag{11}$$

The cost in (11) is convex; however, it is non-differentiable due to the compounded regularization term. This regularizer is such that a closed-form update for $\breve{\mathbf{v}}_g^m[j]$ in general is not

Algorithm 1 ADMM algorithm for solving (11).

Require: Parameters $L_h, \mu, \lambda, \eta > 0$, $\mathbf{w}_g^m[j-1]$, and $\check{\mathbf{v}}_g^{m-1}$.
Randomly initialize $\boldsymbol{\zeta}_g[0]$ and $\boldsymbol{\gamma}_g[0]$.
for $i = 1, \ldots, i_{\max}$ **do**
  Compute $\check{\mathbf{v}}_g[i]$ via (17a).
  Compute $\boldsymbol{\zeta}_g[i]$ via (17b).
  Compute $\boldsymbol{\gamma}_g[i]$ via (16c).
end for

available. Thus, (11) must be solved numerically while bearing in mind that the computational cost associated to each PG iteration hinges on that of solving (11). Note that (11) can be solved in closed form for the special case where $\check{\mathbf{v}}_g^{m-1} = \mathbf{0}_{2F}$, where $\mathbf{0}_{2F}$ is a $2F \times 1$ vector of zeros, and its solution in this case is

$$\check{\mathbf{v}}_g^m[j] = \mathbf{w}_g^m[j-1]\left(1 - \frac{\lambda+\mu}{L_h\|\mathbf{w}_g^m[j-1]\|_2}\right)_+ \quad (12)$$

where $(\cdot)_+ = \max\{0, \cdot\}$.

In order to gain further insight into the solution of (11) when $\check{\mathbf{v}}_g^{m-1} \neq \mathbf{0}_{2F}$, one can use the Karush-Kuhn-Tucker (KKT) conditions combined with the notion of subdifferential to characterize $\check{\mathbf{v}}_g^m[j]$ [3]. With $V^m(\check{\mathbf{v}}_g)$ denoting the cost in (11) and since (11) is an unconstrained optimization problem, the KKT optimality conditions state that $\mathbf{0}_{2F} \in \partial V^m(\check{\mathbf{v}}_g^m[j])$, where $\partial V^m(\check{\mathbf{v}}_g)$ denotes the subdifferential of V^m evaluated at $\check{\mathbf{v}}_g$. The following necessary and sufficient conditions for $\check{\mathbf{v}}_g^m[j]$ follow readily from the optimality condition.

Proposition 2: When $\check{\mathbf{v}}_g^{m-1} \neq \mathbf{0}_{2F}$, the following mutually-exclusive conditions about (11) hold

$$\check{\mathbf{v}}_g^m[j] = \mathbf{0}_{2F} \quad \Leftrightarrow \left\|\mathbf{w}_g^m[j-1] + \alpha_g^{m-1}\check{\mathbf{v}}_g^{m-1}\right\|_2 \leq \frac{\lambda}{L_h} \quad (13a)$$

$$\check{\mathbf{v}}_g^m[j] = \check{\mathbf{v}}_g^{m-1} \Leftrightarrow \left\|\mathbf{w}_g^m[j-1] - \beta_g^{m-1}\check{\mathbf{v}}_g^{m-1}\right\|_2 \leq \frac{\mu}{L_h} \quad (13b)$$

where $\alpha_g^{m-1} = \mu/(L_h\|\check{\mathbf{v}}_g^{m-1}\|_2)$ and $\beta_g^{m-1} = 1 + \lambda/(L_h\|\check{\mathbf{v}}_g^{m-1}\|_2)$.

Prop. 2 can be used to quickly screen whether $\check{\mathbf{v}}^m[j]$ equals $\mathbf{0}_{2F}$ or $\check{\mathbf{v}}^{m-1}$. If neither of these conditions is satisfied, then $\check{\mathbf{v}}^m[j]$ must be obtained by solving (11) numerically.

A. An ADMM-based solver

An efficient iterative solver for (11) based on ADMM is developed in this section. To this end, consider the following optimization problem, which is equivalent to (11),

$$\min_{\check{\mathbf{v}}_g, \boldsymbol{\zeta}_g} \frac{L_h}{2}\left\|\check{\mathbf{v}}_g - \mathbf{w}_g^m[j-1]\right\|_2^2 + \mu\|\check{\mathbf{v}}_g\|_2 + \lambda\|\boldsymbol{\zeta}_g\|_2 \quad (14)$$
$$\text{Subj. to} \quad \boldsymbol{\zeta}_g = \check{\mathbf{v}}_g - \check{\mathbf{v}}_g^{m-1}$$

The ADMM solver for (14) relies on the augmented Lagrangian given by

$$\mathcal{L}(\check{\mathbf{v}}_g, \boldsymbol{\zeta}_g, \boldsymbol{\gamma}_g) = \frac{L_h}{2}\left\|\check{\mathbf{v}}_g - \mathbf{w}_g^m[j-1]\right\|_2^2 + \mu\|\check{\mathbf{v}}_g\|_2 + \lambda\|\boldsymbol{\zeta}_g\|_2$$
$$+ \boldsymbol{\gamma}_g'(\boldsymbol{\zeta}_g - \check{\mathbf{v}}_g + \check{\mathbf{v}}_g^{m-1}) + \frac{\eta}{2}\|\boldsymbol{\zeta}_g - \check{\mathbf{v}}_g + \check{\mathbf{v}}_g^{m-1}\|_2^2 \quad (15)$$

Algorithm 2 PG algorithm for solving (5).

Require: Tuning parameters $\mu, \lambda > 0$ and $\breve{\mathbf{S}}^{m-1}$.
1: **for** $j = 1, 2, \ldots, j_{\max}$ **do**
2:   {These updates can be parallelized}
3:   **for** $g = 1, \ldots, G$ **do**
4:     Compute $\mathbf{w}_g^m[j-1]$ via (9).
5:     **if** $\check{\mathbf{v}}_g^{m-1} = \mathbf{0}_{2F}$ **then**
6:       Update $\check{\mathbf{v}}_g^m[j]$ via (12).
7:     **else if** Condition (13a) is true **then**
8:       Set $\check{\mathbf{v}}_g^m[j] = \mathbf{0}_{2F}$.
9:     **else if** Condition (13b) is true **then**
10:       Set $\check{\mathbf{v}}_g^m[j] = \check{\mathbf{v}}_g^{m-1}$.
11:     **else**
12:       Update $\check{\mathbf{v}}^m[j]$ via Algorithm 1.
13:     **end if**
14:   **end for**
15: **end for**

where $\eta > 0$ is a tuning parameter, and $\boldsymbol{\gamma}_g$ the Lagrange multiplier associated to the equality constraint in (14). With i denoting an iteration index, the ADMM iterations are

$$\check{\mathbf{v}}_g[i] = \arg\min_{\check{\mathbf{v}}_g} \ \mathcal{L}(\check{\mathbf{v}}_g, \boldsymbol{\zeta}_g[i-1], \boldsymbol{\gamma}_g[i-1]) \quad (16a)$$

$$\boldsymbol{\zeta}_g[i] = \arg\min_{\boldsymbol{\zeta}_g} \ \mathcal{L}(\check{\mathbf{v}}_g[i], \boldsymbol{\zeta}_g, \boldsymbol{\gamma}_g[i-1]) \quad (16b)$$

$$\boldsymbol{\gamma}_g'[i] = \boldsymbol{\gamma}_g'[i-1] + \eta\left(\boldsymbol{\zeta}_g[i] - \check{\mathbf{v}}_g[i] + \check{\mathbf{v}}_g^{m-1}\right) \quad (16c)$$

The following proposition shows that updates (16a) and (16b) can be obtained in closed form via soft-thresholding.

Proposition 3: Updates (16a) and (16b) can be performed in closed form as

$$\check{\mathbf{v}}_g[i] = \frac{\boldsymbol{\rho}_g^{m-1}[i-1]}{L_h + \eta}\left(1 - \frac{\mu}{\|\boldsymbol{\rho}_g^{m-1}[i-1]\|_2}\right)_+ \quad (17a)$$

$$\boldsymbol{\zeta}_g[i] = \frac{\boldsymbol{\chi}_g^{m-1}[i-1]}{\eta}\left(1 - \frac{\lambda}{\|\boldsymbol{\chi}_g^{m-1}[i-1]\|_2}\right)_+ \quad (17b)$$

where $\boldsymbol{\rho}_g^{m-1}[i-1] := \eta(\boldsymbol{\zeta}_g[i-1] + \check{\mathbf{v}}_g^{m-1}) + L_h \cdot \mathbf{w}_g^m[j-1] + \boldsymbol{\gamma}_g[i-1]$ and $\boldsymbol{\chi}_g^{m-1}[i-1] := \eta(\check{\mathbf{v}}_g[i] - \check{\mathbf{v}}_g^{m-1}) - \boldsymbol{\gamma}_g[i-1]$.

The resulting ADMM algorithm is summarized as Algorithm 1. Per iteration, its computational complexity is dominated by the evaluation of the Euclidean norms in (17) and it is, thus, $O(F)$. With respect to the convergence of Algorithm 1, note that the sequence $\{\check{\mathbf{v}}_g[i]\}_{i>0}$ does not need to converge to the optimal value of $\check{\mathbf{v}}_g$. Nevertheless, the results in [4, Ch. 3 Prop.4.2] can be used to show that every limit point of $\{\check{\mathbf{v}}_g[i]\}_{i>0}$ corresponds to an optimal solution of (14), and that the sequence $\{\|\boldsymbol{\zeta}_g[i] - \check{\mathbf{v}}_g[i] - \check{\mathbf{v}}_g^{m-1}\|_2\}_{i>0}$ converges to zero, i.e, iterates $\check{\mathbf{v}}_g[i]$ and $\boldsymbol{\zeta}_g[i]$ approach feasibility as $i \to \infty$.

B. The sparse PG tracker

The resulting tracking PG algorithm is summarized as Algorithm 2. In general, its per-iteration computational complexity is dominated by the execution time of Algorithm 1 (line 12). Note, however, that Algorithm 1 is used only

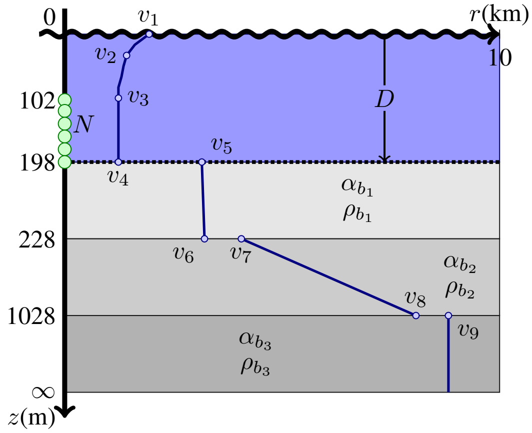

Figure 1. Schematic of the underwater acoustic environmental model used for SWElleX-3. This model is characterized by the compressional sound speeds $\{v_i\}_{i=1}^9$, bottom attenuation coefficients $\{\alpha_{b_i}\}_{i=1}^3$, and bottom densities $\{\rho_{b_i}\}_{i=1}^3$ (shear waves are neglected) [11].

when $\mathbf{v}_g^m[j] \notin \{\mathbf{0}_{2F}, \mathbf{v}_g^{m-1}\}$ and $\mathbf{v}_g^{m-1} \neq \mathbf{0}_{2F}$. Due to the high sparsity regime in which Algorithm 2 operates, few executions of Algorithm 1 are required. When Algorithm 1 is not executed, its computational complexity is dominated by the update in (9) which entails $O(NG)$ operations.

Algorithm 2 can be shown to converge to the solution of (5) while featuring a worst-case convergence rate of $O(1/j)$ [2]. Thus its convergence may be slow in practice, requiring up to several hundreds of iterations to achieve a highly accurate solution. Recent works have shown that it is possible to improve the suboptimal convergence rate of the PG method while maintaining its computational simplicity [2], [12]. These works propose to develop accelerated PG algorithms that feature worst-case convergence rate of $O(1/j^2)$, see [2] and references therein. These algorithmic extensions are not pursued in this paper due to space limitations.

V. Numerical Examples

In this section the performance of the proposed broadband tracking algorithm is illustrated on the third Shallow-Water Evaluation Cell Experiment (SWellEX-3) dataset (see [10] and reference therein for a detailed description of SWellEX-3). In SWellEX-3, a towed source transmitting at frequencies $\{53+16k\}_{k=0}^9$ Hertz and a vertical line array collecting acoustic data were used. In this analysis, only 9 hydrophones, out of 64 hydrophones available, were used. These hydrophones were 11.25 m apart, having a total aperture of 90 m with the bottom element 6 m above the seafloor (water depth was 198 m). A grid with $G = 20,000$ locations spanning radial distances 0-10 km and depths 0-198 m was used. The grid's radial and vertical spacing were 50 m and 2 m, respectively. All replicas were computed with the KRAKEN normal-mode propagation model [13] using the environmental model shown in Fig. 1. Sample parameter values used in the model are: $v_1 = 1,520$ m/s, $v_2 = 1,498$ m/s, $v_3 = 1,490$ m/s, $v_4 = 1,490$ m/s, $v_5 = 1,572$ m/s, $v_6 = 1,593$ m/s, $v_7 = 1,881$ m/s, $v_8 = 3,246$ m/s, $v_9 = 5,200$ m/s, $\alpha_{b_1} = 0.2$ dB/m/kHz, $\alpha_{b_2} = 0.06$ dB/m/kHz, $\alpha_{b_3} = 0.02$ dB/m/kHz, $\rho_{b_1} = 1.76$ g/cm^3, $\rho_{b_2} = 2.06$ g/cm^3, and $\rho_{b_3} = 2.66$ g/cm^3.

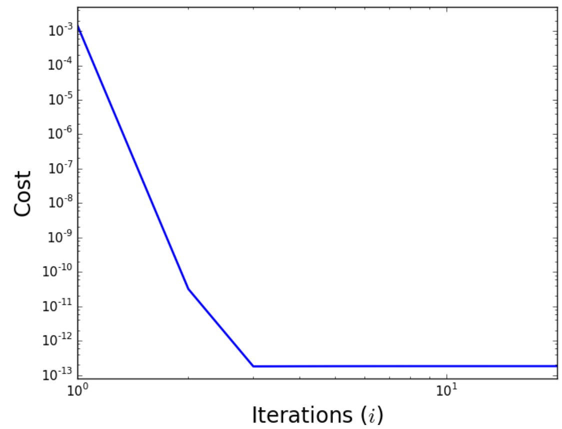

(a) Sample evolution of the cost in (14) when using Algorithm 1 (ADMM).

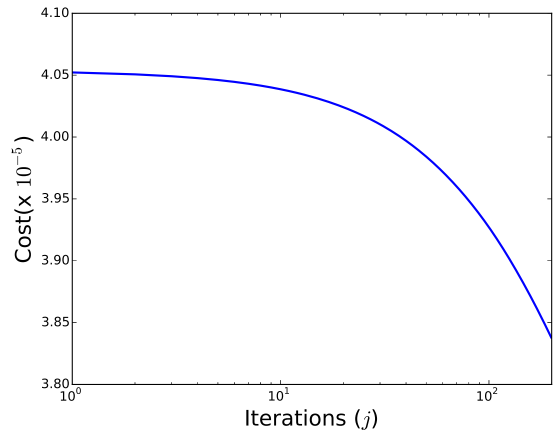

(b) Sample evolution of the cost in (5) when using Algorithm 2 (PG).

Figure 2. Illustration of the cost evolution of the ADMM and PG algorithms.

Fig. 2 illustrates the evolution of the cost of both the ADMM and PG algorithms. Note that ADMM takes few iterations to converge to an acceptable precision. Since ADMM is only used to update few of the $\mathbf{v}_g$'s (in the order of the sparsity of the SLM) per PG iteration, its computational complexity does not significantly affect that of Algorithm 2. On the other hand, the PG algorithm takes a few hundreds of iterations to converge to an acceptable precision as defined by the quality of the source tracks. This motivates future work exploring both predictor screening rules and accelerated PG methods as a mean to reduce the computational complexity of Algorithm 2 both by reducing G and the number of PG iterations required.

Fig. 3 shows the tracks obtained by MFT and Algorithm 2. Despite its high computational complexity, MFT was used as a baseline for constructing the source tracks. A total of

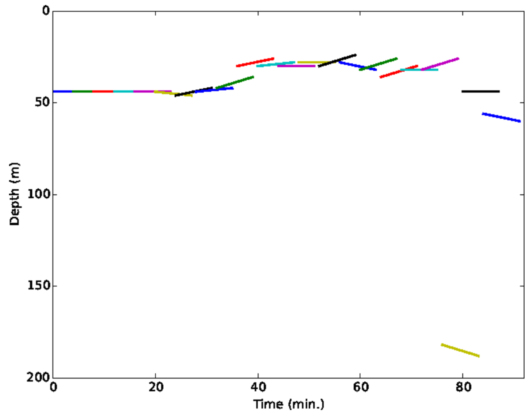

(a) Depth track obtained by MFT.

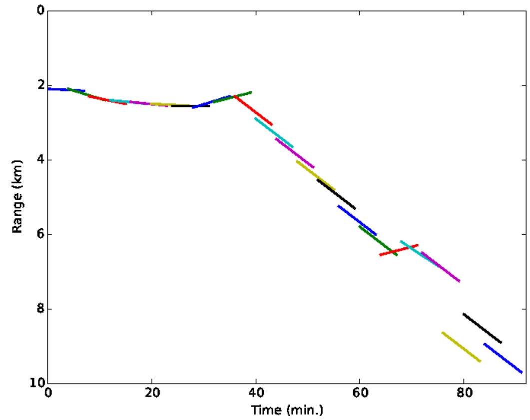

(b) Range track obtained by MFT.

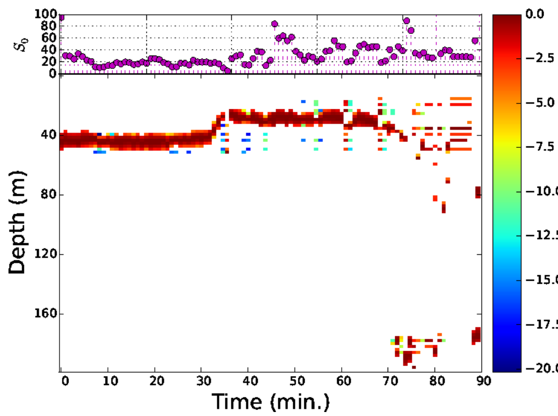

(c) Depth track obtained by Algorithm 2.

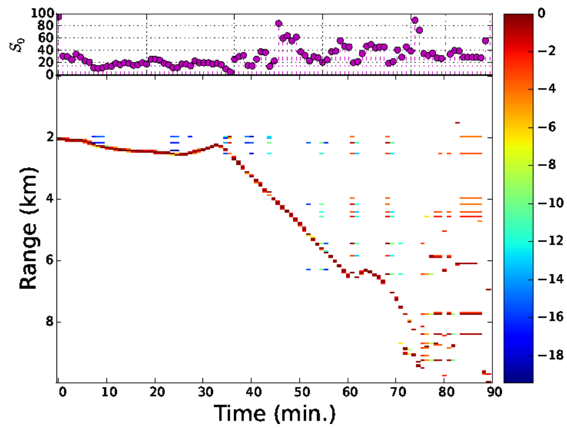

(d) Range Track obtained by Algorithm 2.

Figure 3. Tracks obtained by MFT and Algorithm 2. MFT used a square search window of 22 grid points in range and 5 grid points in depth. The MFT tracks are formed by the short tracks that yielded the largest MFT score. The tracks corresponding to Algorithm 2 show the range and depth of the 10-largest nonzero entries in each SLM. Per SLM, the magnitude of all nonzero entries is normalized with respect to the magnitude of the largest coefficient present.The number of nonzero rows of $\mathbf{S}$, denoted S_0, obtained for each SLM is shown above the tracks.

8 ambiguity surfaces obtained via Bartlett MFP [1], corresponding to 109 seconds of recorded data, were used. Each ambiguity surface accounts for 13.65 seconds of recorded data. MFT tracks were incoherently averaged over frequency. For Algorithm 2, λ and μ were kept fixed for the entire execution of the tracking algorithm. Thus, control on the sparsity of the tracks and the innovations was not exercised. Per time instant, the tracks were constructed by plotting the range and depth of the largest 10 coefficients in the corresponding SLMs. With our selection of tuning parameters, each SLM had 40 nonzero entries on average. When all peaks were plotted to construct the tracks, some artifacts (horizontal lines) appeared in the tracks. These artifacts corresponded to source locations being maintained as part of the track and can be removed by using a dynamic selection scheme for λ and μ. By plotting only the largest 10 coefficients per SLM most of these artifacts are removed. Note that after time index 70, the source reaches an area with significantly different bathymetry. Thus, the difficulty that both MFT and our method have to track the source in the last leg of the track is due to the mismatch between the environment and the model used to construct the replicas. Note that the robust localization framework proposed in [10] can be used within our framework to mitigate the deleterious effect of model mismatch on the source-track estimates.

VI. Conclusions

This work proposed an underwater tracking algorithm using passive sonar that exploits sparsity as a mean to obtain high resolution tracks. Two types of sparsity were exploited, namely sparsity in the support of the SLMs and sparsity in the innovations across consecutive SLMs. The first type of sparsity was motivated by the desideratum of SLMs whose nonzero entries corresponded only to locations where sources were present. The second type of sparsity was motivated by the few changes that occur in the support of consecutive SLMs. Per time instant, an SLM was obtained as the solution of a regularized least-squares problem, where the regularization terms were chosen to encourage the desired sparse structures in each SLM and the innovations. Each SLM is obtained via a computationally efficient proximal gradient algorithm that was tailored to exploit the structure inherent to the problem. Numerical test illustrating the performance of the proposed method on data from SWellEX-3 were presented. From the numerical tests, it was observed that a proper selection of tuning parameters is fundamental to avoid artifacts on the source tracks. Defining a systematic approach for the selection of these parameters was left as an open research direction.

REFERENCES

[1] A. B. Baggeroer, W. A. Kuperman, and P. N. Mikhalevsky, "An overview of matched field methods in ocean acoustics," *IEEE J. Ocean. Eng.*, vol. 18, no. 4, pp. 401–424, 1993.

[2] A. Beck and M. Teboulle, "A fast iterative shrinkage-thresholding algorithm for linear inverse problems," *SIAM Journal on Imaging Sciences*, vol. 2, no. 1, pp. 183–202, 2009.

[3] D. P. Bertsekas, *Nonlinear Programming*, 2nd ed. Athena Scientific, 2009.

[4] D. P. Bertsekas and J. N. Tsitsiklis, *Parallel and Distributed Computation: Numerical Methods*. Athena Scientific, 1997.

[5] H. Bucker, "Matched-field tracking in shallow water," *The Journal of the Acoustical Society of America*, vol. 96, no. 6, pp. 3809–3811, 1994.

[6] A. Charles, M. S. Asif, J. Romberg, and C. Rozell, "Sparsity penalties in dynamical system estimation," in *Proc. of 45th Annual Conference on Information Sciences and Systems (CISS)*, March 2011, pp. 1–6.

[7] S. P. Czenszak and J. L. Krolik, "Robust wideband matched-field processing with a short vertical array," *J. Acoust. Soc. Am.*, vol. 101, no. 2, pp. 749–759, 1997.

[8] S. Farahmand, G. B. Giannakis, G. Leus, and Z. Tian, "Tracking target signal strengths on a grid using sparsity," *EURASIP Journal on Advances in Signal Processing*, vol. 2014, no. 1, 2014.

[9] L. T. Fialkowski, J. S. Perkins, M. D. Collins, M. Nicholas, J. A. Fawcett, and W. Kuperman, "Matched-field source tracking by ambiguity surface averaging," *J. Acoust. Soc. Am.*, vol. 110, no. 2, pp. 739–746, 2001.

[10] P. A. Forero, "Broadband underwater source localization via multitask learning," in *Proc. of 48th Annual Conference on Information Sciences and Systems*, Mar. 19-21, Princeton Univ., Princeton, NJ 2014, pp. 1–6.

[11] F. B. Jensen, W. A. Kuperman, M. B. Porter, and H. Schmidt, *Computational Ocean Acoustics*, 2nd ed. New York, NY, USA: Springer, 2011.

[12] N. Parikh and S. Boyd, "Proximal algorithms," *Found. Trends Optimization*, vol. 1, pp. 123–231, 2013.

[13] M. B. Porter, *The Kraken Normal Mode Program*, SACLANT Undersea Research Centre Memorandum (SM-245) and Naval Research Laboratory Mem. Report 6920, 1991.

[14] M. J. Wilmut, J. M. Ozard, K. O'Keefe, and M. Musil, "A piecewise matched-field tracking algorithm," *IEEE J. Ocean. Eng.*, vol. 23, no. 3, pp. 167–173, Jul. 1998.

[15] M. J. Wilmut, J. M. Ozard, and B. Woods, "An efficient target tracking algorithm for matched field processing," in *Proc. of OCEANS '93. Engineering in Harmony with Ocean*, Oct. 1993, pp. III/81–III/85 vol.3.